Human Molecular Genetics, 2013, Vol. 22, No. 15 **3123–3137**
doi:10.1093/hmg/ddt167
Advance Access published on April 15, 2013

Smooth muscle hyperplasia due to loss of smooth muscle α-actin is driven by activation of focal adhesion kinase, altered p53 localization and increased levels of platelet-derived growth factor receptor-β

Christina L. Papke[1,†], Jiumei Cao[1,†,‡], Callie S. Kwartler[1,†], Carlos Villamizar[1], Katerina L. Byanova[1], Soon-Mi Lim[2], Harini Sreenivasappa[2,3], Grant Fischer[1], John Pham[1], Meredith Rees[1], Miranda Wang[1], Christine Chaponnier[4], Giulio Gabbiani[4], Aarif Y. Khakoo[5], Joya Chandra[6], Andreea Trache[2,3], Warren Zimmer[2] and Dianna M. Milewicz[1,*]

[1]Department of Internal Medicine, University of Texas Health Science Center at Houston, 6431 Fannin, MSB 6.100, Houston, TX 77030, USA, [2]Department of Systems Biology & Translational Medicine, Texas A&M Health Science Center, College Station, TX 77843, USA, [3]Department of Biomedical Engineering, Texas A&M University, College Station, TX 77843, USA, [4]Department of Pathology and Immunology, CMU, University of Geneva, 1211, Switzerland, [5]Metabolic Disorders, Amgen, South San Francisco, CA 94080, USA and [6]Department of Pediatrics Research, University of Texas MD Anderson Cancer Center, Houston, TX 77030, USA

Received December 19, 2012; Accepted April 5, 2013

Mutations in *ACTA2*, encoding the smooth muscle cell (SMC)-specific isoform of α-actin (α-SMA), cause thoracic aortic aneurysms and dissections and occlusive vascular diseases, including early onset coronary artery disease and stroke. We have shown that occlusive arterial lesions in patients with heterozygous *ACTA2* missense mutations show increased numbers of medial or neointimal SMCs. The contribution of SMC hyperplasia to these vascular diseases and the pathways responsible for linking disruption of α-SMA filaments to hyperplasia are unknown. Here, we show that the loss of *Acta2* in mice recapitulates the SMC hyperplasia observed in *ACTA2* mutant SMCs and determine the cellular pathways responsible for SMC hyperplasia. *Acta2*$^{-/-}$ mice showed increased neointimal formation following vascular injury *in vivo*, and SMCs explanted from these mice demonstrated increased proliferation and migration. Loss of α-SMA induced hyperplasia through focal adhesion (FA) rearrangement, FA kinase activation, re-localization of p53 from the nucleus to the cytoplasm and increased expression and ligand-independent activation of platelet-derived growth factor receptor beta (Pdgfr-β). Disruption of α-SMA in wild-type SMCs also induced similar cellular changes. Imatinib mesylate inhibited Pdgfr-β activation and *Acta2*$^{-/-}$ SMC proliferation *in vitro* and neointimal formation with vascular injury *in vivo*. Loss of α-SMA leads to SMC hyperplasia *in vivo* and *in vitro* through a mechanism involving FAK, p53 and Pdgfr-β, supporting the hypothesis that SMC hyperplasia contributes to occlusive lesions in patients with *ACTA2* missense mutations.

INTRODUCTION

Smooth muscle cells (SMCs) contract in response to changes in pulse pressures through cyclic interaction between thin and thick contractile filaments, composed of the SMC-specific isoforms of α-actin (α-SMA) and myosin heavy chain, respectively. Heterozygous mutations in α-SMA, encoded by *ACTA2*, predispose to

*To whom correspondence should be addressed. Tel: +1 7135006715; Fax: +1 7135000693; Email: dianna.m.milewicz@uth.tmc.edu
†The first three authors contributed equally to this work.
‡Present address: Department of Cardiology, Ruijin Hospital, Shanghai Jiaotong University School of Medicine, Shanghai, 200025, PR China.

thoracic aortic aneurysms and acute aortic dissections, along with a variety of occlusive vascular diseases, including early onset coronary artery disease (CAD) and stroke, Moyamoya-like cerebrovascular disease and primary pulmonary hypertension (1–3). Pathology of the occlusive arterial lesions in patients with *ACTA2* mutations shows increased numbers of SMCs in the neointimal or medial layers of the artery, but a paucity of lipid and calcium depositions typically found in atherosclerotic lesions (2,4). Primary cultures of aortic SMCs explanted from patients with *ACTA2* mutations show fewer α-SMA filaments when compared with control SMCs. Additionally, the mutant SMCs proliferate more rapidly when compared with SMCs explanted from donor controls. SMC proliferation occurs during formation of atherosclerotic occlusive lesions, but a role of genetically triggered SMC hyperplasia as a cause of vascular occlusive disease has not been extensively investigated.

A likely axis linking disruption of α-SMA to increased proliferation is the myocardin-related transcription factor-serum response factor (MRTF-SRF) axis, which links the dynamic flux of α-SMA from monomers to filaments with proliferation (5). Unlike myocardin which is constitutively nuclear, MRTFs continuously shuttle between the nucleus and cytoplasm, with localization and activity of MRTFs dependent on cytoplasmic actin polymerization, as well as nuclear import and export mechanisms (6). MRTFs bind monomeric actin and, as actin polymerizes, MRTFs dissociate from actin, unmasking a nuclear localization sequence and facilitating nuclear import via an importin α/β-dependent mechanism (7). In the nucleus, MRTFs bind to the transcriptional co-activator SRF to induce the transcription of SMC contractile genes. As actin filaments are disrupted, monomers accumulate and MRTFs are shuttled out of the nucleus and are sequestered in the cytoplasm by binding to monomeric actin. This leads to the decreased expression of contractile genes, by allowing SRF to bind to ternary complex factors and activate transcription of a subset of SRF-regulated growth responsive genes, such as *Fos* (8,9). Activation of these genes increases the responsiveness of the cells to proliferative cell signaling pathways and growth factors, such as platelet-derived growth factor beta (PDGF-BB).

We sought to determine whether loss of α-SMA leads to SMC hyperplasia and identify the cellular pathways responsible for the increased proliferation. To study cellular proliferation with loss of α-SMA filaments, we chose to examine a mouse model deficient in α-SMA (*Acta2*$^{-/-}$ mice), which was previously reported to have normal vascular development but compromised vascular contractile force, tone and blood flow (10). Aortic SMCs explanted from these mice are hyperplastic *in vitro* and *in vivo*, but the proliferation is not dependent on MRTF-A localization to the cytoplasm. Instead, we found that the cellular pathways contributing to the increased proliferation involve aberrant focal adhesion (FA) localization and activation, leading to altered cellular localization of p53 and increased expression and ligand-independent activation of platelet-derived growth factor receptor beta (Pdgfr-β).

RESULTS

Loss of α-SMA leads to increased SMC proliferation and migration and nuclear localization of MRTF

Aortic SMCs were explanted separately from the ascending and descending aortas of 4-week-old *Acta2*$^{-/-}$ mice since SMCs from these regions of the aorta arise from two different sources, neural crest-derived and mesenchymal-derived progenitor cells, respectively (11). *Acta2*$^{-/-}$ SMCs explanted from both aortic regions proliferated and migrated more rapidly than wild-type (WT) SMCs (Fig. 1A and B, Supplementary Material, Fig. S1A and B). We utilized ascending SMCs for further study because these cells are likely of the same embryonic origin as the SMCs found in occlusive cerebral artery lesions in patients with *ACTA2* mutations, based on the location of these lesions (2).

To determine whether deficiency in α-SMA also increases cellular proliferation in response to vascular injury *in vivo*, we used a flow-cessation injury model of carotid artery to reproducibly induce injury (12). Carotid injury models have been extensively used to study the effects of vascular injury on SMCs and both proliferation and migration of SMCs play a role in the degree of vessel stenosis (12,13). Three weeks post carotid ligation, *Acta2*$^{-/-}$ mice showed exaggerated neointimal formation compared with WT mice based on assessment of the intima/media ratio, neointimal area and percent stenosis of ligated arteries (Fig. 1C). Additionally, labeling of proliferative cells with BrdU and subsequent immunostaining showed an increase in positively stained nuclei in *Acta2*$^{-/-}$ arteries 1 week post ligation (Fig. 1D). Thus, SMC hyperplasia is evident both *in vitro* and *in vivo* with loss of α-SMA.

Acta2$^{-/-}$ aortas were previously reported to have increased α-skeletal actin (encoded by *Acta1*), and *Acta2*$^{-/-}$ pulmonary SMCs were reported to have increased expression of SMC γ-actin (γ-SMA, encoded by *Actg2*) (10,14). We did not detect *Acta1* expression in our *Acta2*$^{-/-}$ SMC explants. However, there was increased *Actg2* mRNA (Fig. 1E). The lack of specific γ-SMA antibodies prevented the assessment of cellular γ-SMA protein levels. Further analysis of actin isoforms in these cells showed no difference in protein levels of β-actin or total actin between mutant and WT SMCs (Fig. 1F, Supplementary Material, Fig. S2A).

To determine whether the MRTF-SRF axis is altered in the *Acta2*$^{-/-}$ SMCs, we assessed the expression levels of contractile genes known to contain CArG boxes and be responsive to MRTF-SRF binding in the promoter region. The *Acta2*$^{-/-}$ SMCs had increased expression of MRTF-SRF-dependent genes, including *Tagln* and *Cnn1* (encoding SM22α and calponin-1, respectively), and corresponding increases in cellular levels of these proteins by immunoblot analysis (Fig. 2A and B). Since MRTF-A is a more potent transcriptional coactivator than MRTF-B in SMCs, MRTF-A cellular location was assessed in the mutant SMCs (5,15). Consistent with increased contractile gene expression, immunofluorescent staining showed increased co-localization of nuclear staining with MRTF-A signal in *Acta2*$^{-/-}$ SMCs compared with WT SMCs (Fig. 2C and D, Supplementary Material, Fig. S2C). Additionally, expression of *Fos*, an SRF-regulated growth responsive gene, was not increased in *Acta2*$^{-/-}$ SMCs (Fig. 2E). Therefore, the hyperplastic *Acta2*$^{-/-}$ SMCs are differentiated, as defined by increased expression of differentiation marker proteins and nuclear MRTF-A localization.

Interestingly, F-to-G actin assays showed no difference in the ratio of total polymerized to unpolymerized actin in the mutant SMCs compared with WT SMCs (Fig. 2F, Supplementary Material, Fig. S2B). However, atomic force microscopy revealed a 2.5-fold increase in local cell stiffness of *Acta2*$^{-/-}$ SMCs (Fig. 2G).

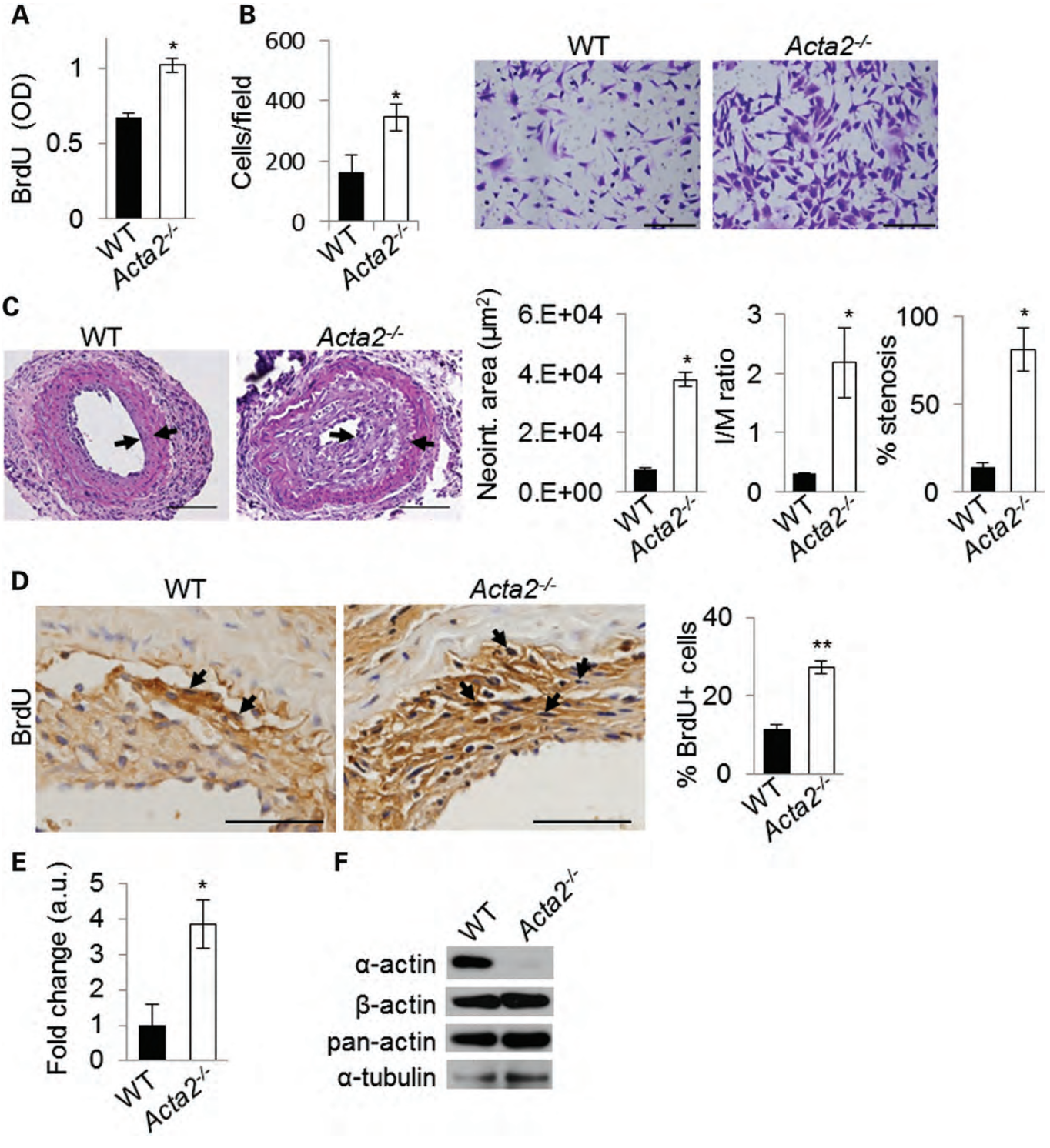

Figure 1. *Acta2*$^{-/-}$ SMCs show increased proliferation and migration *in vitro* and increased proliferation *in vivo* with vascular injury. (**A**) SMCs isolated from ascending aortas of 4-week-old *Acta2*$^{-/-}$ mice show increased proliferation, as quantified by BrdU incorporation, compared with SMCs explanted from WT mice. $^{*}P < 0.05$. Data shown are representative of three independent experiments from three different explants. (**B**) Migration assays were performed using 5 ng/ml PDGF-B as a chemoattractant, and showed increased *Acta2*$^{-/-}$ SMC migration compared with WT SMCs. Five high-powered fields per sample were counted, and data shown are representative of three independent experiments. $^{*}P < 0.05$. Scale bars represent 200 μm. (**C**) Left carotid arteries were ligated and tissue was harvested 3 weeks post injury. Carotid arteries from *Acta2*$^{-/-}$ mice ($n = 7$) showed increased neointimal area, ratio of intimal/medial area and degree of stenosis of the lumen compared with carotid arteries obtained from a similar location in WT mice ($n = 7$). $^{*}P < 0.05$. Arrows denote neointimal layer. Scale bars represent 200 μm. (**D**) Following carotid artery ligation, mice were injected with BrdU 2 h prior to sacrifice. One week post ligation, an increase in BrdU positive nuclei was observed in *Acta2*$^{-/-}$ mice. Top: adventitia. Bottom: neointima. Arrows denote BrdU+ cells. $^{**}P < 0.01$. Scale bars represent 100 μm. (**E**) *Actg2* gene expression was quantified via Q-PCR, and was increased in *Acta2*$^{-/-}$ SMCs. $^{*}P < 0.05$. (**F**) Immunoblotting of β-actin showed similar cytoplasmic actin levels in WT and *Acta2*$^{-/-}$ SMCs. Error bars represent ± SD.

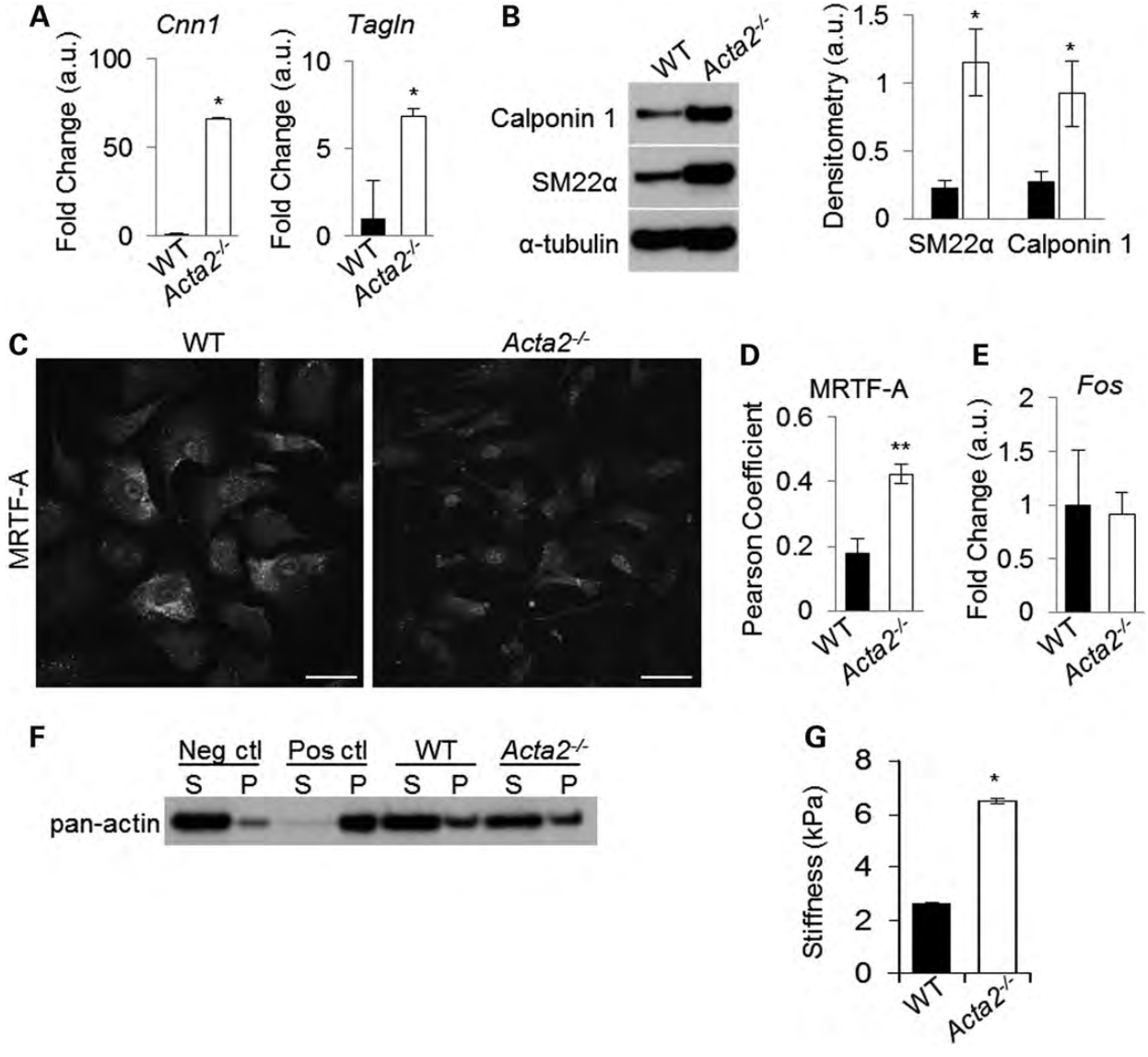

Figure 2. *Acta2*$^{-/-}$ SMCs are not dedifferentiated. (**A**) Contractile gene expression was analyzed using quantitative PCR and showed increased *Cnn1* (calponin-1) and *Tagln* (SM22α) in *Acta2*$^{-/-}$ SMCs compared with WT. $^{*}P < 0.05$. (**B**) Immunoblot analysis showed corresponding increases in calponin-1 and SM22α protein levels in *Acta2*$^{-/-}$ SMCs. Black bars represent WT and white bars represent *Acta2*$^{-/-}$ SMCs. (**C** and **D**) Cells were immunofluorescently labeled with MRTF-A antibody, and nuclear versus cytoplasmic fluorescence was quantified. MRTF-A staining is shown in black-and-white; color panels are included in Supplementary Material, Figure S2C. More MRTF-A is colocalized with nuclear DAPI in *Acta2*$^{-/-}$ SMCs than in the WT cells. Scale bars represent 50 μm. $^{**}P < 0.01$. (**E**) Expression of *Fos*, a gene known to be responsive to changes in MRTF-dependent signaling, was not significantly altered in *Acta2*$^{-/-}$ SMCs compared with WT cells. (**F**) Ultracentrifugation was used to separate supernatant fraction (S) containing G-actin from the pellet fraction (P) containing F-actin. No difference in the ratio of unpolymerized supernatant fraction to polymerized pellet fraction was observed between WT and *Acta2*$^{-/-}$ SMCs. (**G**) Atomic force microscopy was used to quantify cell stiffness. Local cell stiffness is significantly increased in *Acta2*$^{-/-}$ SMCs. $^{*}P < 0.05$. Error bars in (D) represent ±95% CI; all other error bars represent ± SD.

Loss of α-SMA alters FA localization and size, and increases activation of FA kinase

FAs in the *Acta2*$^{-/-}$ SMCs were investigated since increased cellular tension has been shown to drive FA maturation and increased activation of FA-dependent signaling (16), and previous studies identified increased FA kinase (FAK) activity in renal myofibroblasts in *Acta2*$^{-/-}$ mice (17). FA number and size were assessed in the *Acta2*$^{-/-}$ SMCs through immunofluorescence using an anti-vinculin antibody and total internal reflection fluorescence (TIRF) microscopy. These analyses demonstrated redistribution of FAs from dispersion across the cell body to the accumulation at the periphery of the cells, with increased individual FA size but decreased numbers of FAs in *Acta2*$^{-/-}$ SMCs compared with WT SMCs (Fig. 3A and B). In addition to increased FA size, there was increased phosphorylation of FAK at Tyr297 in FAs by TIRF microscopy, indicative of increased FAK activation (Fig. 3A and B). Increased cellular levels of pFAK, along with a corresponding increase in total FAK, were also detected by immunoblot analysis (Fig. 3C). Since FAK is capable of driving Rac1 activation and suppressing RhoA activation (18,19), Rac1 and RhoA activation were

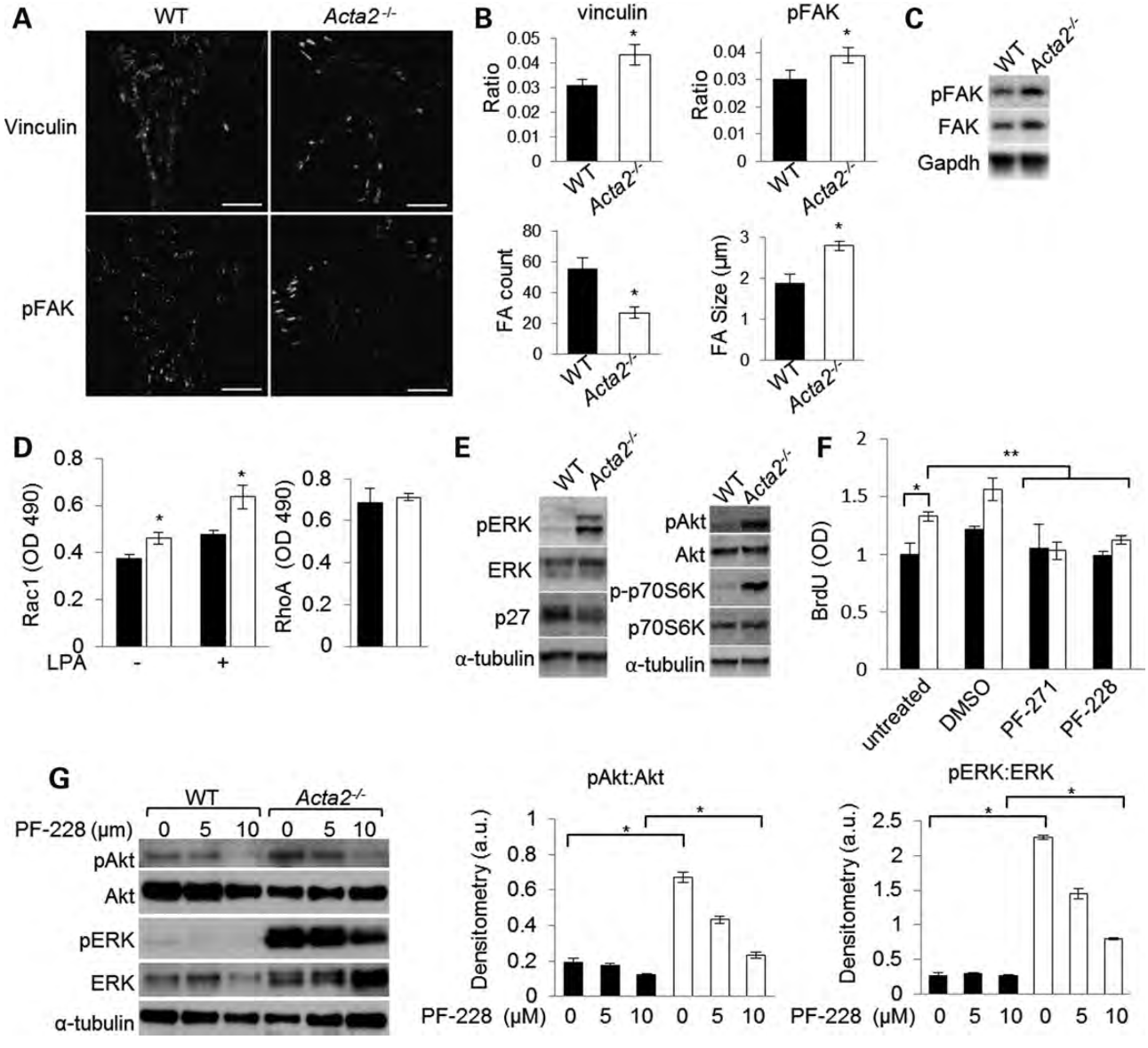

Figure 3. *Acta2*$^{-/-}$ SMC proliferation is in part driven by alterations in FA-dependent signaling. (**A**) Vinculin and pTyr397 FAK were quantified using TIRF microscopy. FAs were localized to the cell periphery in *Acta2*$^{-/-}$ SMCs, whereas FAs were diffusely located across the cell body in the WT cells. Scale bars represent 20 μm. (**B**) TIRF microscopy was used as in (A), and quantification of vinculin, pFAK, FA number and FA size using TIRF microscopy show increased size and vinculin and pFAK content in FAs in *Acta2*$^{-/-}$ SMCs, but a decrease in the overall number of FAs per cell. Data were obtained from at least 10 random cells per each condition using SlideBook software (Intelligent Imaging Innovations, Denver, CO, USA), and were normalized and expressed as a ratio of protein area:cell area. $^{*}P < 0.05$. (**C**) Immunoblotting revealed increased pFAK levels in *Acta2*$^{-/-}$ SMCs. (**D**) G-LISA identified significantly increased Rac1 activation in *Acta2*$^{-/-}$ SMCs, both at baseline and 15 min post stimulation with LPA but no change in RhoA activation. Black bars represent WT and white bars represent *Acta2*$^{-/-}$ SMCs. (**E**) Immunoblots showed increased levels of pAkt and pERK in *Acta2*$^{-/-}$ SMCs. (**F**) Proliferation assays using BrdU incorporation indicate that two distinct FAK inhibitors decreased *Acta2*$^{-/-}$ SMC proliferation to levels similar to WT SMCs. PF-562271 (PF-271) and PF-573228 (PF-228) were each used at a 1 μM concentration. Bars on graph are represented as in (C). Data are representative of at least three independent experiments, and *P*-values were calculated using a Student's *t*-test. $^{*}P < 0.05$. (**G**) Cells were treated with the FAK inhibitor PF-228, and protein lysates were immunoblotted for pERK and pAkt. PF-228 partially blocked ERK and Akt phosphorylation. Bars on graph are represented as in (C). All error bars represent ± SD. $^{*}P < 0.05$.

assessed. There was increased Rac1 activation in *Acta2*$^{-/-}$ SMCs, both without and with stimulation with lysophosphatidic acid [LPA, which induces Rac1 activation in SMCs (20)] as expected, but RhoA activation was not suppressed and remained similar between mutant and WT SMCs (Fig. 3D).

FAK activates multiple downstream pathways that can contribute to cellular proliferation (21,22). Increased phosphorylation of both Akt (pSer473) and ERK1/2 (pThr202/Tyr204) was present in *Acta2*$^{-/-}$ SMCs compared with WT SMCs (Fig. 3E, Supplementary Material, Fig. S3A and B). Additionally, there were increased levels of phosphorylated p70S6 kinase, indicative of mTOR activation, and decreased levels of p27^{kip1}, both of which are cellular changes observed with Akt activation (23) (Fig. 3E, Supplementary Material, Fig. S3A and B).

To determine whether FAK-dependent pathways contribute to the increased proliferation in the mutant SMCs, two different FAK inhibitors, PF-562271 and PF-573228, were used (24,25). Both inhibitors attenuated proliferation of both mutant and WT SMCs and decreased mutant SMC proliferation to the same level as the WT (Fig. 3F). Immunofluorescent staining confirmed that PF-573228 blocked FAK activation (Supplementary Material, Fig. S3C). Interestingly, although the FAK inhibitor decreased proliferation and levels of pFAK in FAs, it only partially blocked ERK1/2 and Akt activation (Fig. 3G).

Loss of α-SMA leads to increased levels of Pdgfr-β and decreased nuclear localization of p53

Activation of Pdgfr-β is a major mitogenic pathway for SMCs and also leads to activation of ERK1/2 and Akt (26). Since the treatment with the FAK inhibitors only partially blocked ERK1/2 and Akt signaling in *Acta2*$^{-/-}$ SMCs, the expression and activation of Pdgfr-β was assessed. *Pdgfrb* gene expression and Pdgfr-β protein levels were significantly increased in *Acta2*$^{-/-}$ SMCs compared with WT SMCs, and there was a corresponding increase in the activation of the receptor as assessed by increased phosphorylation of Tyr1021 (Fig. 4A and B; Supplementary Material, Fig. S4A). Therefore, Pdgfr-β signaling is increased in *Acta2*$^{-/-}$ SMCs due to the increased levels of the receptor. To determine whether there was also increased stability of Pdgfr-β protein in the mutant cells, *Acta2*$^{-/-}$ and WT SMCs were exposed to cycloheximide to block protein translation for various time points up to 8 h. Pdgfr-β levels decreased more rapidly in the WT than mutant cells, suggesting that Pdgfr-β was degraded more slowly in the mutant cells (Supplementary Material, Fig. S4B). Thus, in *Acta2*$^{-/-}$ SMCs, *Pdgfrb* transcript and Pdgfr-β protein levels are increased, and the protein is more stable than in WT SMCs.

Treatment with either the FAK inhibitor PF-573228 or the mTOR inhibitor rapamycin significantly attenuated Pdgfr-β expression at both the mRNA and protein levels (Fig. 4C and D; Supplementary Material, Fig. S4C). In contrast, inhibition of ERK1/2 did not alter *Pdgfrb* expression (data not shown). The tumor suppressor p53 is a known transcriptional repressor of *Pdgfrb* expression in other cell types. Studies in cancer cells have shown that either FAK or mTOR activation can alter p53; FAK activation decreases p53 activity, and mTOR activation decreases nuclear localization of p53 (27–30). Assessment of the localization of cellular p53 by immunofluorescence indicated localization predominantly in the nucleus in WT SMCs, but primarily cytoplasmic localization in *Acta2*$^{-/-}$ SMCs. Treatment with the FAK or mTOR inhibitor decreased cytoplasmic and increased nuclear p53 in *Acta2*$^{-/-}$ SMCs (Fig. 4G). The ability of a pharmaceutical activator of p53, CP-31398 (31), to repress *Pdgfrb* expression and alter p53 cellular localization was also assessed. CP-31398 decreased *Pdgfrb* gene expression and Pdgfr-β protein levels in *Acta2*$^{-/-}$ SMCs after 4 h at a dose of 15 μg/ml with no evidence of toxicity (31) (Fig. 4E and F, Supplementary Material, Fig. S4D). CP-31398 also increased the intensity of p53 staining throughout the cell and significantly increased the ratio of nuclear to cytoplasmic staining of p53 (Fig. 4G). CP-31398 completely inhibited all cellular proliferation in both *Acta2*$^{-/-}$ and WT SMCs (data not shown). These data suggest that in *Acta2*$^{-/-}$ SMCs, a mechanism involving FAK and mTOR activation re-localized p53 to the cytoplasm, leading to increased *Pdgfrb* expression and protein levels.

Pdfgr-β activation in *Acta2*$^{-/-}$ SMCs is ligand independent and influenced by cellular reactive oxygen species levels, and drives *Acta2*$^{-/-}$ SMCs proliferation *in vitro* and *in vivo*

Neutralizing antibody and conditioned media experiments were performed to determine whether the increased Pdgfr-β activation in the *Acta2*$^{-/-}$ SMCs was ligand dependent. Exogenous PDGF-BB increased Pdgfr-β activation, and pretreatment with PDGF-BB neutralizing antibody completely prevented the PDGF-BB-induced increase as reported by others but did not further reduce Pdgfr-β activation in the *Acta2*$^{-/-}$ SMCs (32). Additionally, incubation with the antibody failed to decrease Pdgfr-β activation in untreated *Acta2*$^{-/-}$ SMCs. Conditioned media from *Acta2*$^{-/-}$ SMCs did not increase Pdgfr-β activation in WT SMCs, providing further evidence supporting ligand-independent activation of Pdgfr-β in *Acta2*$^{-/-}$ SMCs (Fig. 5A and B; Supplementary Material, Fig. S5A and B).

Increased cellular reactive oxygen species (ROS) have been shown to promote ligand-independent activation of Pdgfr-β by inhibiting the protein tyrosine phosphatase responsible for de-phosphorylating the activated receptor (33,34). Additionally, Rac1 activation has been associated with increased ROS production in SMCs (35). To determine whether ROS contribute to Pdgfr-β activation in *Acta2*$^{-/-}$ SMCs, we quantified ROS levels by staining *Acta2*$^{-/-}$ SMCs with MitoSOX, a fluorescent probe for mitochondrial ROS production. Flow cytometry showed significantly higher fluorescent signal in *Acta2*$^{-/-}$ SMCs than the WT, indicating increased ROS (Fig. 5C). The flavoenzyme inhibitor diphenyleneiodonium (DPI) was able to inhibit Pdgfr-β activation in a dose-dependent manner in *Acta2*$^{-/-}$ SMCs and also blocked cellular proliferation at a dose of 5 μM (Fig. 5D, Supplementary Material, Fig. S5E). In addition, both rotenone and antimycin A, which block mitochondrial respiratory complexes I and III, respectively, attenuated Pdgfr-β activation and proliferation in *Acta2*$^{-/-}$ SMCs (Supplementary Material, Fig. S5C and D).

Acta2$^{-/-}$ SMCs were exposed to imatinib to determine whether blocking tyrosine kinase receptor activation could attenuate proliferation. Treatment with 10 μM imatinib decreased proliferation of *Acta2*$^{-/-}$ SMCs to the level of WT SMCs (Fig. 5E). Immunoblot analysis confirmed that imatinib effectively blocked phosphorylation of Pdgfr-β (Supplementary Material, Fig. S5F). To determine the role of Pdgfr-β in neointimal formation *in vivo*, daily intraperitoneal injections of imatinib (50 mg/kg/day) were given after carotid artery ligation. Imatinib effectively blocked neointimal formation after carotid artery injury in *Acta2*$^{-/-}$ mice, but also blocked neointimal formation in the WT mice as has previously been reported in other systems (36) (Fig. 5F).

An α-SMA disrupting peptide induces phenotypic changes in WT SMCs similar to *Acta2*$^{-/-}$ SMCs

To determine whether disruption of α-SMA filaments in WT SMCs leads to FA alterations, altered p53 cellular localization and increased expression of Pdgfr-β, we used a cell-permeable peptide that disrupts α-SMA filament formation (αSMA-fp)

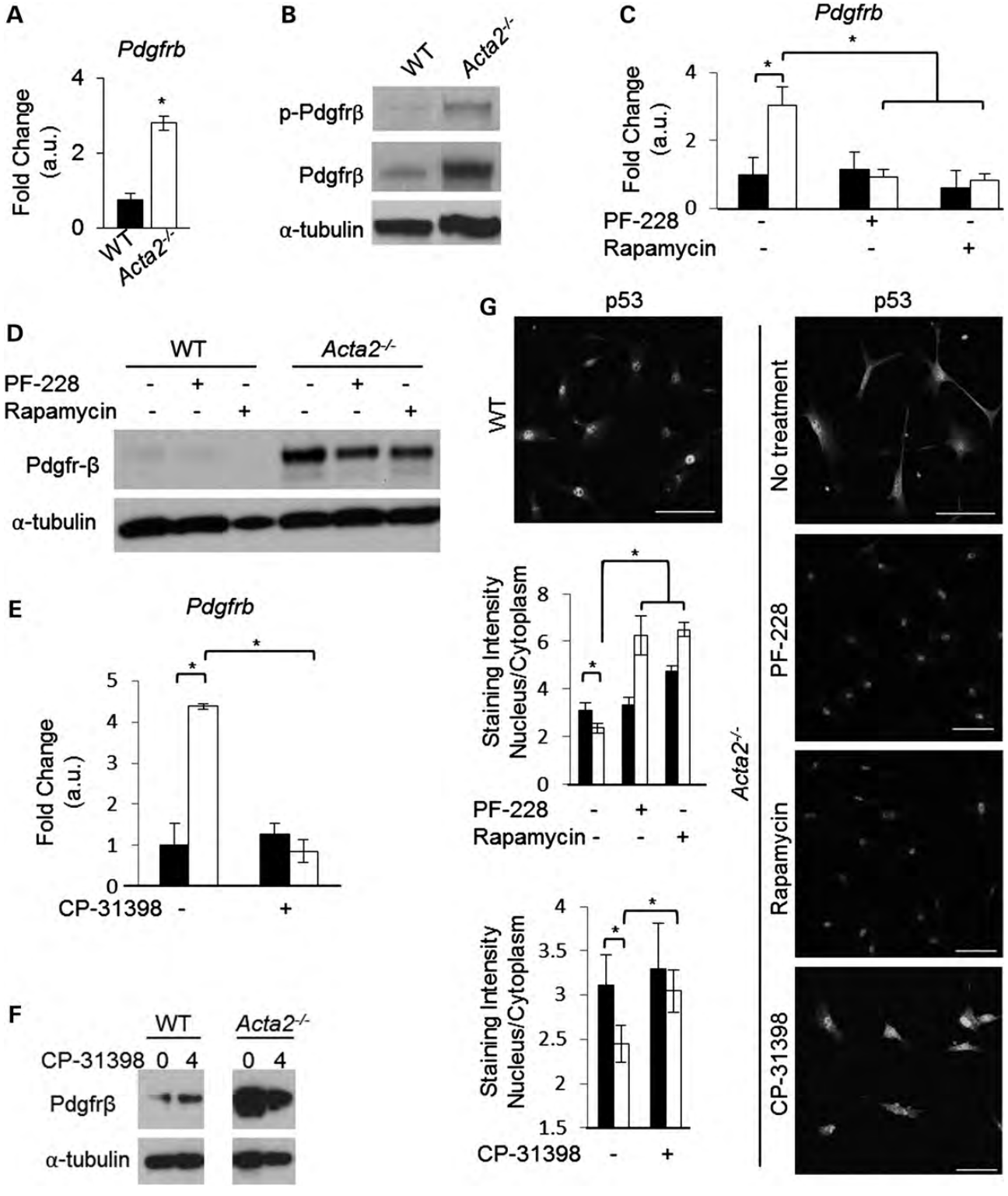

Figure 4. Increased Pdgfr-β expression and stability in *Acta2*$^{-/-}$ SMCs. (**A**) Quantitative PCR showed increased *Pdgfrb* gene expression in *Acta2*$^{-/-}$ SMCs. $^{*}P < 0.05$. (**B**) Immunoblots showed increased Pdgfr-β protein expression and phosphorylation at Tyr1021 in *Acta2*$^{-/-}$ SMCs. (**C** and **D**) Cells were treated with either mTOR inhibitor (rapamycin) or FAK inhibitor (PF-228). Treatment with either inhibitor significantly reduced *Pdgfrb* gene (C) and Pdgfr-β protein (D) expression in *Acta2*$^{-/-}$ SMCs. $^{*}P < 0.05$. Black bars represent WT and white bars represent *Acta2*$^{-/-}$ SMCs. (**E** and **F**) Cells were treated with an activator of p53, CP-31398. *Pdgfrb* gene (E) and Pdgfr-β protein (F) expression were significantly reduced in *Acta2*$^{-/-}$ SMCs following CP-31398 treatment. $^{*}P < 0.05$. Bars on graph are represented as in (C). (**G**) Cells were immunofluorescently labeled using a p53 antibody. p53 is localized predominantly in the nucleus in WT SMCs, but predominantly in the cytoplasm in *Acta2*$^{-/-}$ SMCs. Treatment with rapamycin, FAK inhibitor or p53 activator drives p53 back into the nucleus in *Acta2*$^{-/-}$ SMCs. $^{*}P < 0.05$. Bars on graph are represented as in (C).

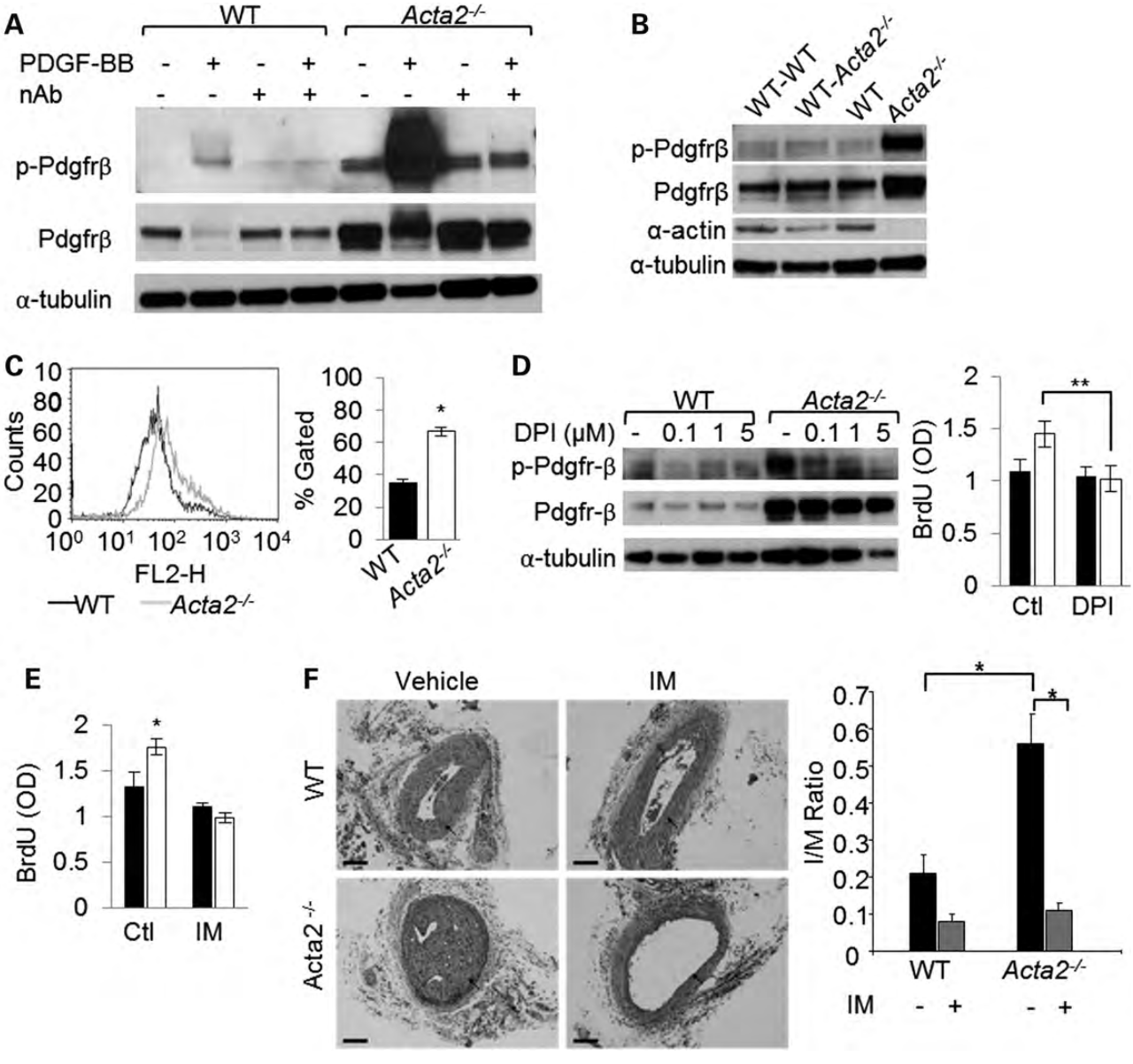

Figure 5. Pdgfr-β activation in *Acta2*$^{-/-}$ SMCs is ligand-independent, regulated in part by ROS, and a contributor to *Acta2*$^{-/-}$ SMC hyperplasia *in vitro* and *in vivo*. (**A**) Cells were treated with a neutralizing antibody against PDGF-BB (1 μg/ml). Neutralizing antibody treatment effectively blocked PDGF-BB (20 ng/ml) induced receptor phosphorylation but failed to reduce baseline receptor activation in *Acta2*$^{-/-}$ SMCs. (**B**) WT cells were incubated with conditioned media from either WT or *Acta2*$^{-/-}$ SMCs. *Acta2*$^{-/-}$ conditioned media failed to activate Pdgfr-β in WT SMCs. An equivalent amount of cell lysate from untreated *Acta2*$^{-/-}$ SMCs was used as a positive control. (**C**) Cells were trypsinized, incubated with a MitoSOX probe for 20 min to label mitochondrial ROS and subjected to flow cytometric analysis. Mitochondrial-derived ROS levels were increased in *Acta2*$^{-/-}$ SMCs. (**D**) Cells were treated with NADPH oxidase inhibitor (DPI). DPI treatment reduced Pdgfr-β phosphorylation in *Acta2*$^{-/-}$ SMCs and blocked proliferation of *Acta2*$^{-/-}$ SMCs at a dose of 5 μM. (**E**) Imatinib mesylate (IM) at a dose of 10 μM decreased *Acta2*$^{-/-}$ SMC proliferation *in vitro* to levels similar to WT SMCs. $^{*}P < 0.05$. Black bars represent WT and white bars represent *Acta2*$^{-/-}$ SMCs. (**F**) Left carotid arteries in mice were ligated, and harvested 21 days post injury. Mice were given either vehicle or imatinib mesylate (50 mg/kg/day) 2 h prior to injury and once per day thereafter. Imatinib completely prevents neointimal formation in both WT and *Acta2*$^{-/-}$ arteries. Black arrows indicate the border between the medial and neointimal layers. $n = 6$ mice per experimental group. Black bars on graph represent vehicle treated and grey bars represent imatinib treated mice. $^{*}P < 0.05$. Scale bars represent 200 μm. All error bars represent ± SD.

and a control peptide that disrupts α skeletal actin (α-SKA) but not α-SMA filaments (αSKA-fp) (37). Immunofluorescence analysis of α-SMA filaments and total actin filaments was performed on WT SMCs following 24 h of peptide treatment. Cells exposed to αSKA-fp had minimal loss of α-SMA filaments when compared with control SMCs, whereas SMCs treated with αSMA-fp showed no α-SMA filaments and no pools of monomeric α-SMA (Fig. 6A, Supplementary Material, Fig. S6A). Immunofluorescence of FAs using an anti-vinculin antibody showed localization of FAs to the cell periphery in the αSMA-fp treated cells but not in the αSKA-fp treated cells (Fig. 6A and B, Supplementary Material, Fig. S6B). Staining

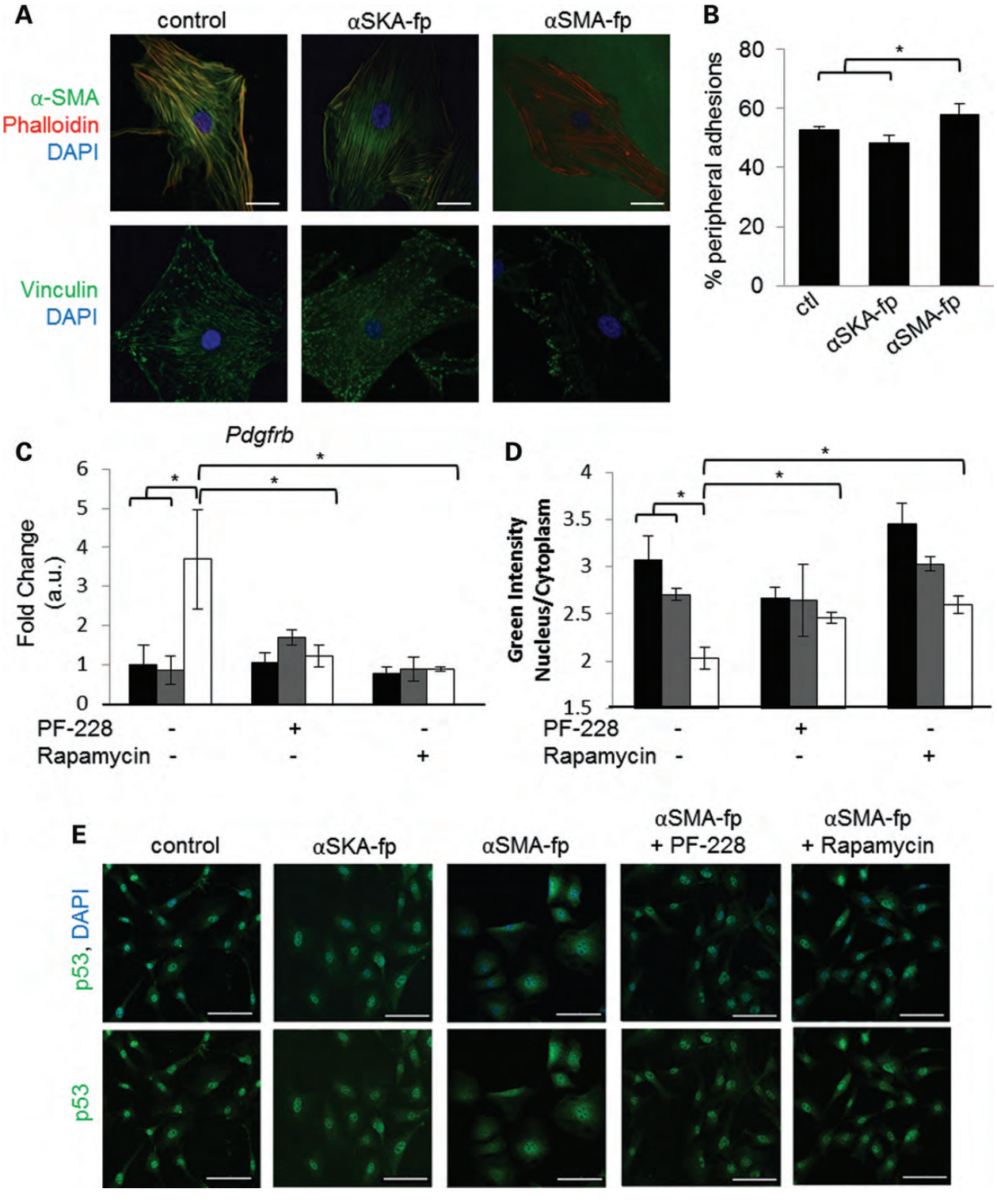

Figure 6. A peptide that disrupts α-SMA filaments in cells leads to FA relocalization to the periphery and increased *Pdgfrb* gene expression in WT SMCs. (**A**–**E**). WT cells were treated with either an SMA-disrupting peptide (αSMA-fp) or control peptide targeting skeletal α-actin (αSKA-fp) and harvested for analysis. (A) Immunostaining of α-SMA showed that actin filaments are disrupted 24 h after addition of 1 μg/ml αSMA-fp as opposed to no disruption in untreated cells or cells treated with 1 μg/ml αSKA-fp. The increased green background in the αSMA-fp-treated cells is most likely due to cross-reaction of the α-SMA antibody with the αSMA-fp peptide. Immunostaining with an anti-vinculin antibody showed relocalization of the FAs to the periphery of the interface between the cell and the culture dish in αSMA-fp-treated SMCs. Scale bars represent 20 μm. (B) The number of FAs was quantified, and showed a difference in adhesion localization between SKA-fp and SMA-fp-treated WT SMCs. $^{*}P < 0.05$. (C) Q-PCR data showing increased *Pdgfrb* gene expression 24 h after adding αSMA-fp but not αSKA-fp. Treatment with either PF-228 or rapamycin rescued this increased expression. $^{*}P < 0.05$. Combined data from three independent experiments are shown. Black bars represent WT untreated, grey bars represent SKA-fp treated and white bars represent SMA-fp-treated cells. All error bars represent ± SEM. (D and E) Quantitation (D) and images (E) showing altered cellular localization of p53 after treatment with SMA-fp but not SKA-fp. This change is rescued by treatment with either PF-228 or rapamycin. Bars on graph are represented as in (C). $^{*}P < 0.05$. Scale bars represent 100 μm.

for MRTF-A revealed that, similar to the *Acta2*$^{-/-}$ SMCs, cells treated with the αSMA-fp peptide have increased nuclear localization of MRTF-A (Supplementary Material, Fig. S7A and B). Furthermore, disruption of α-SMA filaments in WT SMCs with αSMA-fp led to significantly increased *Pdgfrb* gene expression (Fig. 6C). Co-treatment with αSMA-fp and an inhibitor of FAK (PF-228) or of mTOR (rapamycin) blocked the increase in *Pdgfrb* expression associated with α-SMA disruption by the peptide (Fig. 6C). Immunofluorescence staining for p53 confirmed that treatment with αSMA-fp, but not αSKA-fp, reduced the nuclear localization of p53, and inhibition of either FAK or mTOR blocked this decrease in nuclear localization with αSMA-fp treatment (Fig. 6D and E). The serum starvation required for peptide treatment affected the ability to assess proliferation after peptide treatment; however, the αSMA-fp treated cells but not the αSKA-fp treated cells show a reproducible and marginally statistically significant increase in BrdU incorporation (Supplementary Material, Fig. S6C). The combination of serum deprivation and CP-31398 treatment caused cell death; therefore, we were unable to confirm increased nuclear localization of p53 with CP-31398 treatment. Thus, disruption of the α-SMA filaments in WT SMCs leads to altered FAs, increased *Pdgfrb* expression and cytoplasmic p53 localization, recapitulating the phenotypic features of the *Acta2*$^{-/-}$ SMCs.

DISCUSSION

We previously observed decreased α-SMA filaments and increased proliferation in SMCs explanted from patients with *ACTA2* mutations (2). Furthermore, occlusive vascular lesions in these patients are characterized by increased numbers of medial or intimal SMCs. The results presented here demonstrate that loss of α-SMA filaments in a mouse model increases SMC proliferation *in vitro* and leads to excessive neointimal formation with vascular injury *in vivo*. Although the carotid ligation model used in this study is not directly translatable into a pathological process in humans, it does provide a well-established, useful model for studying the proliferative response of *Acta2*$^{-/-}$ SMCs to vascular injury (12,13,38). Thus, these data support the hypothesis that a hyperplastic response of the SMCs contributes to the increased risk of occlusive vascular diseases in patients with *ACTA2* mutations. Coronary arteries from patients with *ACTA2* mutations display lesions with minimal lipid and calcium deposits but enriched in SMCs, suggesting that SMC hyperplasia may represent an alternative molecular pathway from a single gene mutation to CAD. It is also important to note that recent studies have implicated a similar role of genetically triggered SMC hyperplasia in CAD in the general population. A locus on 9p21 harbors genetic polymorphisms that increased the risk for CAD (39) and deletion of an orthologous region in mice caused excessive aortic SMC proliferation (40). Further studies are needed to confirm the molecular basis of the atherosclerotic risk associated with the 9p21 locus; however, our data presented here also support a role for a genetically triggered hyperplastic response of SMCs in the pathogenesis of occlusive vascular diseases.

The *Acta2*$^{-/-}$ SMCs proliferate more rapidly than WT SMCs and display a phenotype divergent from the classical definition of dedifferentiated SMCs, specifically increased expression of contractile protein with MRTF-A localized to the nucleus and increased SMC proliferation. Previously, evidence of adult SMC phenotypes divergent from the canonical differentiated versus proliferative cells as defined by the MRTF-SRF axis have been postulated but poorly described (41). Dedifferentiated SMCs in advanced atherosclerotic lesions have been shown to exhibit low rates of proliferation (42), and loss of Krüppel-like factor 4 inhibits both SMC differentiation and proliferation (43). During development, vascular SMC precursors are highly proliferative while expressing increasing amounts of SMC-specific contractile proteins (44). The data presented here support that adult mouse SMCs can assume a simultaneously proliferative and differentiated phenotype and provide a cellular mechanism by which SMCs assume this phenotype.

Surprisingly, despite the loss of α-SMA, there was not a significant change in the amount of total actin expression, and cellular tension was increased. The loss of α-SMA increased the expression of *Actg2* and total cellular actin levels remained unchanged when compared with WT SMCs. The γ-SMA isoform is predominant in the gut, where visceral SMCs undergo phasic contraction, and γ-actin isoforms in particular have been shown to be more dynamic than other isoforms during muscle contraction (45). The substitution of γ-SMA for α-SMA, in conjunction with increased expression of other contractile proteins driven by MRTF transcriptional activity, could be responsible for the increased cell stiffness. It is important to note that increased *Actg2* expression in *Acta2*$^{-/-}$ SMCs was documented, but we were not able to confirm increased γ-SMA protein levels in these SMCs due to the lack of a specific γ-SMA antibody. However, based on the data showing that the loss of α-SMA is not associated with decreased total cellular actin levels, we can conclude that the protein levels of other actin isoforms are increased, and the increased expression of *Actg2* suggests that γ-SMA is one of the isoforms increased.

Deficiency of α-SMA and increased stiffness in *Acta2*$^{-/-}$ SMCs was associated with altered localization of FAs at the cell periphery, enlargement of the FAs based on vinculin content and excessive activation of FAK when compared with WT cells (Fig. 7). Following formation of nascent FAs at the cell periphery, the enlargement and maturation of FAs are dependent on further force generation by the cell (46,47). In myofibroblasts, FA maturation has been demonstrated to specifically require α-SMA force generation (48). Furthermore, both α-SMA expression and functional, force-generating actin filaments are required for assembly and maturation of FAs in cells, a process driven by FAK (48–50). Our data suggest instead that the loss of α-SMA leads to the formation of FAs with increased size and continued FAK activation. The increase in cell stiffness in *Acta2*$^{-/-}$ SMCs is consistent with these findings; increased cell stiffness has been shown to correspond with an increase in both cytoskeletal tension and FA size, leading to the formation of so-called supermature FAs (51). Interestingly, these 'supermature' FAs in *Acta2*$^{-/-}$ SMCs were also associated with increased activation of Rac1, but no change in activation of RhoA. Rac1 and RhoA are usually reciprocally regulated. For example, when smooth muscle myosin motor function is disrupted by a missense mutation in the motor domain, *MYH11* R247C, the SMCs have smaller FAs, with increased Rac1 and decreased RhoA activation (52). The loss

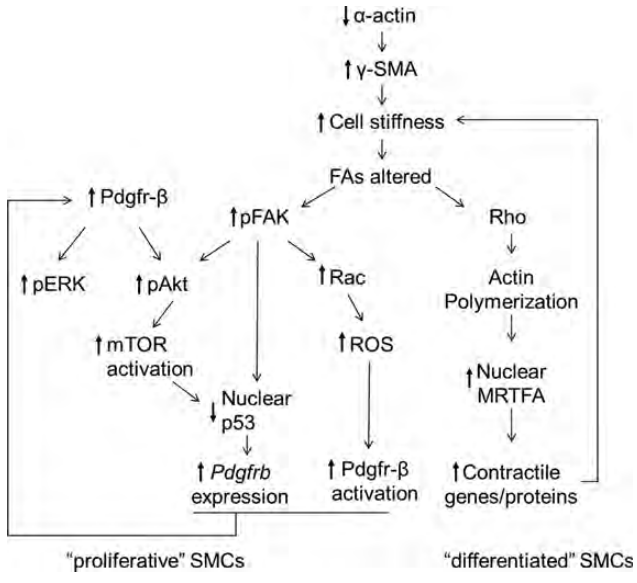

Figure 7. Proposed mechanisms by which loss of α-actin increases proliferation and Pdgfr-β expression without inducing SMC dedifferentiation.

of RhoA activation decreases actin polymerization and therefore MRTF-A is cytoplasmic localized, and the cells assume a dedifferentiated phenotype. Other cellular changes in the *Acta2*$^{-/-}$ SMCs, such as increased mTOR signaling or decreased p27^{kip1} levels, have previously been reported to increase the activation of cellular RhoA and may contribute to maintaining RhoA activity in the *Acta2*$^{-/-}$ SMCs (53,54).

In addition to FAK activation, the *Acta2*$^{-/-}$ SMCs displayed increased expression and activation of Pdgfr-β, and increased cytoplasmic localization of p53 when compared with WT SMCs. The tumor suppressor p53 has previously been identified as a transcriptional repressor of *Pdgfrb* in cancer cells (29). We further determined that inhibition of either FAK or mTOR suppressed the expression of *Pdgfrb* and restored the nuclear localization of p53 in *Acta2*$^{-/-}$ SMCs. Previous studies have reported a direct interaction between FAK and p53 in cancer cells (55). This interaction was mapped to a region of FAK that includes the major phosphorylation site required for FAK activation, tyrosine 397 (56). Additionally, it has also been shown that inhibition of mTOR leads to p53 re-localization from the cytoplasm to the nucleus in multiple cancer cell lines (30). We were also able to show that a p53-activating drug suppressed *Pdgfrb* expression and re-localized p53 from the cytoplasm to the nucleus in *Acta2*$^{-/-}$ SMCs. All these data suggest that in *Acta2*$^{-/-}$ SMCs, excessive activation of FAK and/or mTOR leads to p53 re-localization from the nucleus to the cytoplasm and increased expression of *Pdgfrb* (Fig. 7). Further studies are need to confirm that p53 represses *Pdgfrb* transcription in SMCs and determine specific mechanisms by which increased FAK and mTOR activation in the *Acta2*$^{-/-}$ SMCs results in the altered cellular localization of p53.

Our data utilizing a peptide that specifically disrupts α-SMA filaments suggest that these pathways are directly relevant to human patients with *ACTA2* mutations, who have disruption rather than loss of α-SMA filaments. Peptide treatment was chosen over siRNA knockdown since α-SMA is present but not formed properly into filaments in *ACTA2* mutant SMCs. SMCs exposed to the disrupting peptide recapitulated many of the phenotypic changes in the *Acta2*$^{-/-}$ SMCs, including altered FA localization, reduced nuclear localization of p53 and increased *Pdgfrb* gene expression. The *ACTA2* mutations identified in families with thoracic aortic disease and occlusive vascular lesions are primarily missense mutations predicted to produce mutant α-SMA monomers, and this was confirmed via immunofluorescence (1,2). Based on our current understanding, we hypothesize that mutant α-SMA will alter filament formation and force generation, and consequently lead to activation of the same proliferative pathways identified in the *Acta2*$^{-/-}$ SMCs (2). If the *ACTA2* missense mutations disrupt α-SMA filament polymerization or stability, there may additionally be increased pools of monomeric actin available to bind MRTF-A in the cytoplasm, allowing SRF to bind to growth responsive genes and further drive proliferation.

The proliferative pathways identified in *Acta2*$^{-/-}$ SMCs are remarkably similar to well-studied proliferative pathways in malignant cancer cells. Our findings raise the possibility that targeted chemotherapeutic drugs blocking proliferative pathways in cancer cells may be beneficial to patients with occlusive vascular disease caused by hyperplastic SMCs. Increased proliferation of *Acta2*$^{-/-}$ SMCs was attenuated *in vitro* by both FAK inhibitors and a protein tyrosine kinase inhibitor, suggesting that proliferation was driven by both pathways. Since PDGF-BB is a major mitogen for SMCs and is increased *in vivo* with vascular injury, we selected imatinib for a treatment trial to block SMC proliferation in neointimal lesions in the *Acta2*$^{-/-}$ mice. Imatinib prevented neointimal formation in these mice at a dose lower than that used to reduce tumor growth in mice (50 mg/kg/day compared with 150 mg/kg/day) (57,58). Interestingly, imatinib blocked neointimal formation in both the mutant and WT mice. Long-term treatment using imatinib for chronic myelogenous leukemia and gastrointestinal stromal tumors has shown that this drug can be given for years with few serious side effects (59). Imatinib can also block proliferation in classically de-differentiated populations of SMCs explanted from porcine coronary arteries (60). Imatinib trials are currently in progress for pulmonary hypertension, another arterial occlusive disease due to hyperproliferative SMCs, and these trials have shown initial improvement in hemodynamics and functional lung capacity (61,62). Future studies will determine whether imatinib therapy may also be beneficial in preventing or limiting the occlusive vascular lesions in patients with *ACTA2* mutations.

MATERIALS AND METHODS

Mice

All mouse experiments were carried out in accordance with institutional guidelines at The University of Texas at Houston for the care and use of animals. Standard methods were used to rederive *Acta2*$^{-/-}$ mice from frozen embryos obtained from Dr Warren Zimmer at Texas A&M University. Mice were originally generated by Schildmeyer *et al*. (10) and were subsequently bred onto a C57 background for ≥ 10 generations.

SMC isolation and culture

SMCs were explanted from the ascending and descending aortas of age- and gender-matched *Acta2*$^{-/-}$ and WT littermates as previously described (38). Cells were subcultured in Smooth Muscle Basal Media containing 20% FBS, pyruvate, HEPES, L-glutamine, antibiotic and growth factors (SmBM Bullet Kit; Lonza). Following initial experiments, ascending SMCs were utilized for the remainder of the studies, and all SMCs were plated on dishes coated with Type IV collagen (Sigma). Cells were serum starved for 24 h in culture media with 1% FBS and all other supplements except growth factors prior to analysis. Cells from at least three separate explants were analyzed with similar results, and cells for all experiments were serum-starved in SmBM containing 1% FBS for 24 h prior to treatment unless otherwise noted. Cell culture assays were performed in triplicate, and data shown are representative of at least three independent experiments.

Immunofluorescence

SMCs were seeded at a density of 5000 cells per 22 mm round cover slip and allowed to attach overnight. Following serum starvation, cover slips were fixed with either 4% paraformaldehyde in 0.1 M phosphate buffer or methanol–acetone (50/50%). Cells were permeabilized in 0.1% Triton X-100 for 10 min and blocked for 1 h in 5% normal donkey serum, incubated with primary antibodies overnight at 4°C and secondary antibodies for 1 h at room temperature. Primary antibodies were obtained from Millipore (p397FAK, 1:50), BD Biosciences (p397FAK, 1:200), Sigma (α-SMA, 1:100; vinculin, 1:200; vinculin-FITC, 1:500) and Santa Cruz (MRTF-A, 1:50; p53, 1:50). Secondary antibodies and fluorophores were purchased from Jackson Immunoresearch, Vector Labs and Invitrogen. High-resolution confocal images were obtained using a Nikon A1R confocal microscope, and quantifications were performed using NIS Elements software (Nikon).

TIRF microscopy

For quantification of FA proteins, TIRF microscopy was utilized to excite fluorescent proteins within ~90 nm of the plasma membrane. The inverted Olympus IX-81 microscope with a TIRF attachment is described in Trache & Lim (2009) (63). A PLAN APO 60X oil 1.45 NA objective lens was used to acquire images. We used SlideBook software (Intelligent Imaging Innovations) to measure the FA area and total cell area for each image. The ratio of FA area to total cell area was calculated for each cell as previously described in Lim *et al.* (64), and quantitative data from 10 cells from each condition were pooled.

Immunoblotting and quantitative PCR

Cells plated at equal density were lysed in RIPA buffer containing phosphatase and protease inhibitors. Total protein quantification and immunoblotting were performed using standard protocols. Antibodies used for immunoblotting were obtained from Cell Signal (p-ERK1/2, ERK1/2, Pdgfr-β, p-p70S6K, p70S6K, p-Akt, Akt; all at 1:1000 dilution), Millipore (p397FAK, 1:750), Santa Cruz (FAK, 1:500; pY1021 Pdgfr-β, 1:500;), Abcam (α-tubulin, 1:1000), Fitzgerald (Gapdh, 1:20,000), Sigma (α-SMA, 1:5000; β-actin, 1:1000; SM 22α, 1:1000) and Novus Biologicals (Calponin-1, 1:1000). Immunoblots were analyzed using ImageJ software (NIH). RNA was isolated using Tri Reagent (Sigma). CDNA synthesis was performed using Multiscribe reverse transcriptase and random primers, and quantitative PCR was performed using Taqman assays according to the manufacturer's instructions. All quantitative PCR reagents were purchased from Applied Biosystems. For protein stability assays, SMCs were treated with cyclohexamide (50 μg/ml), harvested at the indicated time points and analyzed by immunoblotting.

Carotid artery ligation and *in vivo* inhibitor treatment

Carotid artery ligations were performed on 8-week-old WT and *Acta2*$^{-/-}$ mice. Mice were anesthetized using intraperitoneal injection of 2.5% avertin. The left common carotid artery was ligated near its bifurcation with the use of 5-0 silk sutures. Animal survival was > 95%. The mice were allowed to survive 21 days post ligation. Two hours before sacrifice, mice were injected intraperitoneally with BrdU (Sigma B-5002). For morphological analysis, animals were perfused with normal saline and fixed with 10% buffered formalin at physiologic pressure for 3 min. Left and right carotid arteries were removed, further fixed in 10% buffered formalin for 16 h and paraffin-embedded without further dissection. The entire length of the left and right carotid arteries was sectioned and examined for identification of the site with most significant stenosis. Carotid artery tissues were stained using standard protocols. Specimens were imaged and photographed using an Olympus microscope. For morphometric analyses, images of H&E stained cross-sections of injured and control arteries were analyzed using Image J (NIH). Perimeters of the lumen, internal elastic lamina (IEL) and external elastic lamina (EEL) were obtained by tracing the contours on digitized images using ImageJ software. Intimal thickness (distance between lumen and IEL) and medial thickness (distance between IEL and EEL) were calculated. Percent lumen stenosis was calculated as: (intima area/IEL area) × 100. For imatinib mesylate treatment, 50 mg/kg imatinib in dimethyl sulfoxide (DMSO) or DMSO alone (vehicle) was administered once intraperitoneally at 4 h following injury, and once daily for 14 days post injury. Carotid arteries were harvested for histology 21 days post injury.

Cell proliferation and migration assays

SMCs were seeded at a density of 5000 cells/well in 96-well microplates and allowed to attach overnight. Cells were pretreated for 30 min in SmBM containing 1% FBS with either vehicle (DMSO) or the indicated inhibitors before addition of BrdU, and incubated with BrdU for 24 h. BrdU ELISAS were performed according to the manufacturer's instructions (Millipore). Assays were performed in triplicate, and graphs are representative of at least three independent experiments.

A modified Boyden chamber assay was used to quantify cell migration. A total of 50 000 SMCs were seeded in duplicate into polycarbonate filters (BD Biosciences) fitted into 24-well plates, with a pore size of 8×10^{-3} mm. The bottom chamber contained 5 ng/ml PDGF-B as a chemoattractant. Cells were

incubated for 6 h before gently scraping any unmigrated cells from the upper surface of the porous membrane and visualizing migrated cells with 0.5% Crystal Violet. Stained membranes were mounted onto slides and a blinded observer photographed five random 400x fields from each membrane. The number of migratory cells was counted, and results were expressed as mean ± SD, representative of at least three independent experiments.

αSKA-fp and αSMA-fp peptide experiments

WT SMCs were seeded onto cover slips as previously described. After incubation of cells in SmBM containing 1% FBS for 24 h, cells were treated with 10 ng/ml TGF-β1. Forty-eight hours post TGF-β1 treatment, cells were incubated with 1 μg/ml of either αSKA-fp or αSMA-fp for 24 h in Owens media. Both peptides have been previously characterized by Hinz *et al.* (37). Controls were treated with Owens media alone. Drug treatments were added at the same time as peptide. Immunofluorescence was performed as described above using antibodies against α-SMA, vinculin, MRTF-A and p53; cells were imaged using a Nikon A1 confocal microscope, and images were quantified using NIS Elements software. For analysis of *Pdgfrb* expression, quantitative PCR was carried out as described above.

Flow cytometry

Intracellular ROS levels were quantified using flow cytometry. Cells were seeded onto collagen IV coated plates, incubated overnight and serum starved in SmBM with 1% FBS. Cells were then trypsinized and labeled with Mitosox red (5 μM) for 20 min Probes were washed out using PBS, and cells were resuspended in PBS for reading on a flow cytometer. Data were analyzed using CellQuest Pro and Kaluza software.

G-LISA

Cells were seeded and serum starved as previously described. Cells were harvested in the provided lysis buffer and snap-frozen in liquid nitrogen, and G-LISAs for RhoA and Rac1 were carried out according to the manufacturer's instructions (Cytoskeleton, cat. no. BK-124 and BK-128).

F-to-G actin assays

Cells were seeded and serum starved as previously described. The ratio of F-to-G actin was determined using an ultracentrifugation method and kit from Cytoskeleton. Cells were harvested in F-actin lysis buffer and ultracentrifuged according to the manufacturer's instructions. Equal volumes of supernatant (containing G-actin) and pellet (containing F-actin) fractions were electrophoresed, and semi-quantitative analysis was performed via immunoblotting.

Atomic force microscopy

To determine the stiffness of the cell at the point of contact, the atomic force microscope (AFM) was operated in force mode. An uncoated AFM probe (MLCT, Bruker Nano-Surfaces) was driven to touch and retract from the cell surface over a known predefined distance in the z-axis.

The z-axis movement and the deflection signal from the probe were recorded in a force curve (65). The force curve was analyzed using Sneddon's modified Hertz model to obtain the Young modulus of elasticity at the point of contact (66,67). All force curves were acquired at a position midway between the nucleus and the edge of the cell. Measurements were performed for 2 min per cell, and repeated for more than 10 cells in two different experiments. Thus, over 2000 force curves were acquired in Nanoscope software (Bruker Nano-Surfaces Inc.) for each sample. The force curves were processed off-line using NForceR software [Trzeciakowski JP, Meininger GA. NForceR: nanoscale force reader and AFM data analysis package (copyrighted), 2004] followed by PeakFit software (SYSTAT Software Inc.) analysis.

Statistical analysis

Data were analyzed using Student's *t*-tests or two-way ANOVA, with *P*-values ≤ 0.05 considered statistically significant.

SUPPLEMENTARY MATERIAL

Supplementary Material is available at HMG online.

Conflict of Interest statement. A.Y.K. is a full-time employee of Amgen, Inc.

FUNDING

This work was supported by NIH (P50HL083794-01, R01 HL62594, and P01 HL110869 to D.M.M.); The Swiss National Science Foundation (310030_125320 to C.C.); The National Marfan Foundation Victor A. McKusick Fellowship to (C.L.P.); The Whitaker Foundation (D.M.M.); Richard T. Pisani Funds (D.M.M.); the Alpha Omega Alpha Carolyn L. Kuckein Student Research Fellowship to (J.P.); the NSF CAREER award (0747334 to A.T.); the American Heart Association National Scientist Development Grant (0835205N to A.T.); and The Center for Clinical and Translational Sciences, funded by National Institutes of Health Clinical and Translational Award from the National Center for Research Resources (UL1 RR024148).

REFERENCES

1. Guo, D.C., Pannu, H., Papke, C.L., Yu, R.K., Avidan, N., Bourgeois, S., Estrera, A.L., Safi, H.J., Sparks, E., Amor, D. *et al.* (2007) Mutations in smooth muscle alpha-actin (*ACTA2*) lead to thoracic aortic aneurysms and dissections. *Nat. Genet.*, **39**, 1488–1493.
2. Guo, D.C., Papke, C.L., Tran-Fadulu, V., Regalado, E.S., Avidan, N., Johnson, R.J., Kim, D.H., Pannu, H., Willing, M.C., Sparks, E. *et al.* (2009) Mutations in smooth muscle alpha-actin (ACTA2) cause coronary artery disease, stroke, and moyamoya disease, along with thoracic aortic disease. *Am. J. Hum. Genet.*, **84**, 617–627.
3. Milewicz, D.M., Ostergaard, J.R., la-Kokko, L.M., Khan, N., Grange, D.K., Mendoza-Londono, R., Bradley, T.J., Olney, A.H., Ades, L., Maher, J.F. *et al.* (2010) De novo ACTA2 mutation causes a novel syndrome of multisystemic smooth muscle dysfunction. *Am. J. Med. Genet. A.*, **152**, 2437–2443.
4. Stary, H.C., Chandler, A.B., Dinsmore, R.E., Fuster, V., Glagov, S., Insull, W. Jr, Rosenfeld, M.E., Schwartz, C.J., Wagner, W.D. and Wissler, R.W. (1995) A definition of advanced types of atherosclerotic lesions and a

histological classification of atherosclerosis. A report from the Committee on Vascular Lesions of the Council on Arteriosclerosis, American Heart Association. *Arterioscler. Thromb. Vasc. Biol.*, **15**, 1512–1531.
5. Parmacek, M.S. (2007) Myocardin-related transcription factors: critical coactivators regulating cardiovascular development and adaptation. *Circ. Res.*, **100**, 633–644.
6. Vartiainen, M.K., Guettler, S., Larijani, B. and Treisman, R. (2007) Nuclear actin regulates dynamic subcellular localization and activity of the SRF cofactor MAL. *Science*, **316**, 1749–1752.
7. Pawlowski, R., Rajakyla, E.K., Vartiainen, M.K. and Treisman, R. (2010) An actin-regulated importin alpha/beta-dependent extended bipartite NLS directs nuclear import of MRTF-A. *EMBO J.*, **29**, 3448–3458.
8. Posern, G., Sotiropoulos, A. and Treisman, R. (2002) Mutant actins demonstrate a role for unpolymerized actin in control of transcription by serum response factor. *Mol. Biol. Cell*, **13**, 4167–4178.
9. Zaromytidou, A.I., Miralles, F. and Treisman, R. (2006) MAL and ternary complex factor use different mechanisms to contact a common surface on the serum response factor DNA-binding domain. *Mol. Cell Biol.*, **26**, 4134–4148.
10. Schildmeyer, L.A., Braun, R., Taffet, G., Debiasi, M., Burns, A.E., Bradley, A. and Schwartz, R.J. (2000) Impaired vascular contractility and blood pressure homeostasis in the smooth muscle alpha-actin null mouse. *FASEB J.*, **14**, 2213–2220.
11. Majesky, M.W. (2007) Developmental basis of vascular smooth muscle diversity. *Arterioscler. Thromb. Vasc. Biol.*, **27**, 1248–1258.
12. Kumar, A. and Lindner, V. (1997) Remodeling with neointima formation in the mouse carotid artery after cessation of blood flow. *Arterioscler. Thromb. Vasc. Biol.*, **17**, 2238–2244.
13. Xu, J., Ismat, F.A., Wang, T., Yang, J. and Epstein, J.A. (2007) NF1 regulates a Ras-dependent vascular smooth muscle proliferative injury response. *Circulation*, **116**, 2148–2156.
14. Shardonofsky, F.R., Moore, J., Schwartz, R.J. and Boriek, A.M. (2012) Airways in smooth muscle alpha-actin null mice experience a compensatory mechanism that modulates their contractile response. *J. Appl. Physiol.*, **112**, 898–903.
15. Shen, D., Li, J., Lepore, J.J., Anderson, T.J., Sinha, S., Lin, A.Y., Cheng, L., Cohen, E.D., Roberts, J.D. Jr, Dedhar, S. *et al.* (2011) Aortic aneurysm generation in mice with targeted deletion of integrin-linked kinase in vascular smooth muscle cells. *Circ. Res.*, **109**, 616–628.
16. Goffin, J.M., Pittet, P., Csucs, G., Lussi, J.W., Meister, J.J. and Hinz, B. (2006) Focal adhesion size controls tension-dependent recruitment of alpha-smooth muscle actin to stress fibers. *J. Cell Biol.*, **172**, 259–268.
17. Takeji, M., Moriyama, T., Oseto, S., Kawada, N., Hori, M., Imai, E. and Miwa, T. (2006) Smooth muscle alpha-actin deficiency in myofibroblasts leads to enhanced renal tissue fibrosis. *J. Biol. Chem.*, **281**, 40193–40200.
18. Chang, F., Lemmon, C.A., Park, D. and Romer, L.H. (2007) FAK potentiates Rac1 activation and localization to matrix adhesion sites: a role for betaPIX. *Mol. Biol. Cell*, **18**, 253–264.
19. Ren, X.D., Kiosses, W.B., Sieg, D.J., Otey, C.A., Schlaepfer, D.D. and Schwartz, M.A. (2000) Focal adhesion kinase suppresses Rho activity to promote focal adhesion turnover. *J. Cell Sci.*, **113**(Pt 20), 3673–3678.
20. Kaneyuki, U., Ueda, S., Yamagishi, S., Kato, S., Fujimura, T., Shibata, R., Hayashida, A., Yoshimura, J., Kojiro, M., Oshima, K. and Okuda, S. (2007) Pitavastatin inhibits lysophosphatidic acid-induced proliferation and monocyte chemoattractant protein-1 expression in aortic smooth muscle cells by suppressing Rac-1-mediated reactive oxygen species generation. *Vascul. Pharmacol.*, **46**, 286–292.
21. Gilmore, A.P. and Romer, L.H. (1996) Inhibition of focal adhesion kinase (FAK) signaling in focal adhesions decreases cell motility and proliferation. *Mol. Biol. Cell*, **7**, 1209–1224.
22. Parsons, J.T. (2003) Focal adhesion kinase: the first ten years. *J. Cell Sci.*, **116**, 1409–1416.
23. Sedding, D.G., Seay, U., Fink, L., Heil, M., Kummer, W., Tillmanns, H. and Braun-Dullaeus, R.C. (2003) Mechanosensitive p27Kip1 regulation and cell cycle entry in vascular smooth muscle cells. *Circulation*, **108**, 616–622.
24. Slack-Davis, J.K., Martin, K.H., Tilghman, R.W., Iwanicki, M., Ung, E.J., Autry, C., Luzzio, M.J., Cooper, B., Kath, J.C., Roberts, W.G. and Parsons, J.T. (2007) Cellular characterization of a novel focal adhesion kinase inhibitor. *J. Biol. Chem.*, **282**, 14845–14852.
25. Roberts, W.G., Ung, E., Whalen, P., Cooper, B., Hulford, C., Autry, C., Richter, D., Emerson, E., Lin, J., Kath, J. *et al.* (2008) Antitumor activity and pharmacology of a selective focal adhesion kinase inhibitor, PF-562,271. *Cancer Res.*, **68**, 1935–1944.
26. Inui, H., Kitami, Y., Tani, M., Kondo, T. and Inagami, T. (1994) Differences in signal transduction between platelet-derived growth factor (PDGF) alpha and beta receptors in vascular smooth muscle cells. PDGF-BB is a potent mitogen, but PDGF-AA promotes only protein synthesis without activation of DNA synthesis. *J. Biol. Chem.*, **269**, 30546–30552.
27. Ilic, D., Almeida, E.A., Schlaepfer, D.D., Dazin, P., Aizawa, S. and Damsky, C.H. (1998) Extracellular matrix survival signals transduced by focal adhesion kinase suppress p53-mediated apoptosis. *J. Cell Biol.*, **143**, 547–560.
28. Nigro, J.M., Aldape, K.D., Hess, S.M. and Tlsty, T.D. (1997) Cellular adhesion regulates p53 protein levels in primary human keratinocytes. *Cancer Res.*, **57**, 3635–3639.
29. Yang, W., Wetterskog, D., Matsumoto, Y. and Funa, K. (2008) Kinetics of repression by modified p53 on the PDGF beta-receptor promoter. *Int. J. Cancer*, **123**, 2020–2030.
30. Mungamuri, S.K., Yang, X., Thor, A.D. and Somasundaram, K. (2006) Survival signaling by Notch1: mammalian target of rapamycin (mTOR)-dependent inhibition of p53. *Cancer Res.*, **66**, 4715–4724.
31. Takimoto, R., Wang, W., Dicker, D.T., Rastinejad, F., Lyssikatos, J. and el-Deiry, W.S. (2002) The mutant p53-conformation modifying drug, CP-31398, can induce apoptosis of human cancer cells and can stabilize wild-type p53 protein. *Cancer Biol. Ther.*, **1**, 47–55.
32. Kwapiszewska, G., Markart, P., Dahal, B.K., Kojonazarov, B., Marsh, L.M., Schermuly, R.T., Taube, C., Meinhardt, A., Ghofrani, H.A., Steinhoff, M. *et al.* (2012) PAR-2 inhibition reverses experimental pulmonary hypertension. *Circ. Res.*, **110**, 1179–1191.
33. Saito, S., Frank, G.D., Mifune, M., Ohba, M., Utsunomiya, H., Motley, E.D., Inagami, T. and Eguchi, S. (2002) Ligand-independent trans-activation of the platelet-derived growth factor receptor by reactive oxygen species requires protein kinase C-delta and c-Src. *J. Biol. Chem.*, **277**, 44695–44700.
34. Kappert, K., Sparwel, J., Sandin, A., Seiler, A., Siebolts, U., Leppanen, O., Rosenkranz, S. and Ostman, A. (2006) Antioxidants relieve phosphatase inhibition and reduce PDGF signaling in cultured VSMCs and in restenosis. *Arterioscler. Thromb. Vasc. Biol.*, **26**, 2644–2651.
35. Patil, S., Bunderson, M., Wilham, J. and Black, S.M. (2004) Important role for Rac1 in regulating reactive oxygen species generation and pulmonary arterial smooth muscle cell growth. *Am. J. Physiol. Lung Cell Mol. Physiol*, **287**, L1314–L1322.
36. Makiyama, Y., Toba, K., Kato, K., Hirono, S., Ozawa, T., Saigawa, T., Minagawa, S., Isoda, M., Asami, F., Ikarashi, N. *et al.* (2008) Imatinib mesilate inhibits neointimal hyperplasia via growth inhibition of vascular smooth muscle cells in a rat model of balloon injury. *Tohoku J. Exp. Med.*, **215**, 299–306.
37. Hinz, B., Gabbiani, G. and Chaponnier, C. (2002) The NH2-terminal peptide of alpha-smooth muscle actin inhibits force generation by the myofibroblast in vitro and in vivo. *J. Cell Biol.*, **157**, 657–663.
38. Cao, J., Gong, L., Guo, D.C., Mietzsch, U., Kuang, S.Q., Kwartler, C.S., Safi, H., Estrera, A., Gambello, M.J. and Milewicz, D.M. (2010) Thoracic aortic disease in tuberous sclerosis complex: molecular pathogenesis and potential therapies in Tsc2+/- mice. *Hum. Mol. Genet.*, **19**, 1908–1920.
39. McPherson, R., Pertsemlidis, A., Kavaslar, N., Stewart, A., Roberts, R., Cox, D.R., Hinds, D.A., Pennacchio, L.A., Tybjaerg-Hansen, A., Folsom, A.R. *et al.* (2007) A common allele on chromosome 9 associated with coronary heart disease. *Science*, **316**, 1488–1491.
40. Visel, A., Zhu, Y., May, D., Afzal, V., Gong, E., Attanasio, C., Blow, M.J., Cohen, J.C., Rubin, E.M. and Pennacchio, L.A. (2010) Targeted deletion of the 9p21 non-coding coronary artery disease risk interval in mice. *Nature*, **464**, 409–412.
41. Owens, G.K. (1995) Regulation of differentiation of vascular smooth muscle cells. *Physiol. Rev.*, **75**, 487–517.
42. Gordon, D., Reidy, M.A., Benditt, E.P. and Schwartz, S.M. (1990) Cell proliferation in human coronary arteries. *Proc. Natl Acad. Sci. USA*, **87**, 4600–4604.
43. Yoshida, T., Kaestner, K.H. and Owens, G.K. (2008) Conditional deletion of Kruppel-like factor 4 delays downregulation of smooth muscle cell differentiation markers but accelerates neointimal formation following vascular injury. *Circ. Res.*, **102**, 1548–1557.
44. Lee, S.H., Hungerford, J.E., Little, C.D. and Iruela-Arispe, M.L. (1997) Proliferation and differentiation of smooth muscle cell precursors occurs simultaneously during the development of the vessel wall. *Dev. Dyn.*, **209**, 342–352.

45. Kim, H.R., Gallant, C., Leavis, P.C., Gunst, S.J. and Morgan, K.G. (2008) Cytoskeletal remodeling in differentiated vascular smooth muscle is actin isoform dependent and stimulus dependent. *Am. J. Physiol. Cell Physiol.*, **295**, C768–C778.
46. Burridge, K. and Chrzanowska-Wodnicka, M. (1996) Focal adhesions, contractility, and signaling. *Annu. Rev. Cell Dev. Biol.*, **12**, 463–518.
47. Choi, C.K., Vicente-Manzanares, M., Zareno, J., Whitmore, L.A., Mogilner, A. and Horwitz, A.R. (2008) Actin and alpha-actinin orchestrate the assembly and maturation of nascent adhesions in a myosin II motor-independent manner. *Nat. Cell Biol.*, **10**, 1039–1050.
48. Hinz, B., Dugina, V., Ballestrem, C., Wehrle-Haller, B. and Chaponnier, C. (2003) Alpha-smooth muscle actin is crucial for focal adhesion maturation in myofibroblasts. *Mol. Biol. Cell*, **14**, 2508–2519.
49. Ronnov-Jessen, L. and Petersen, O.W. (1996) A function for filamentous alpha-smooth muscle actin: retardation of motility in fibroblasts. *J. Cell Biol.*, **134**, 67–80.
50. Geiger, B. and Bershadsky, A. (2001) Assembly and mechanosensory function of focal contacts. *Curr. Opin. Cell Biol.*, **13**, 584–592.
51. Wang, N., Tolic-Norrelykke, I.M., Chen, J., Mijailovich, S.M., Butler, J.P., Fredberg, J.J. and Stamenovic, D. (2002) Cell prestress. I. Stiffness and prestress are closely associated in adherent contractile cells. *Am. J. Physiol. Cell Physiol.*, **282**, C606–C616.
52. Kuang, S.Q., Kwartler, C.S., Byanova, K.L., Pham, J., Gong, L., Prakash, S.K., Huang, J., Kamm, K.E., Stull, J.T., Sweeney, H.L. and Milewicz, D.M. (2012) Rare, nonsynonymous variant in the smooth muscle-specific isoform of myosin heavy chain, MYH11, R247C, alters force generation in the aorta and phenotype of smooth muscle cells. *Circ. Res.*, **110**, 1411–1422.
53. Liu, L., Luo, Y., Chen, L., Shen, T., Xu, B., Chen, W., Zhou, H., Han, X. and Huang, S. (2010) Rapamycin inhibits cytoskeleton reorganization and cell motility by suppressing RhoA expression and activity. *J. Biol. Chem.*, **285**, 38362–38373.
54. Besson, A., Gurian-West, M., Schmidt, A., Hall, A. and Roberts, J.M. (2004) p27Kip1 modulates cell migration through the regulation of RhoA activation. *Genes Dev.*, **18**, 862–876.
55. Golubovskaya, V.M., Finch, R. and Cance, W.G. (2005) Direct interaction of the N-terminal domain of focal adhesion kinase with the N-terminal transactivation domain of p53. *J. Biol. Chem.*, **280**, 25008–25021.
56. Golubovskaya, V.M., Finch, R., Zheng, M., Kurenova, E.V. and Cance, W.G. (2008) The 7-amino-acid site in the proline-rich region of the N-terminal domain of p53 is involved in the interaction with FAK and is critical for p53 functioning. *Biochem. J.*, **411**, 151–160.
57. Schultheis, B., Nijmeijer, B.A., Yin, H., Gosden, R.G. and Melo, J.V. (2012) Imatinib mesylate at therapeutic doses has no impact on folliculogenesis or spermatogenesis in a leukaemic mouse model. *Leuk. Res.*, **36**, 271–274.
58. Wolff, N.C. and Ilaria, R.L. Jr (2001) Establishment of a murine model for therapy-treated chronic myelogenous leukemia using the tyrosine kinase inhibitor STI571. *Blood*, **98**, 2808–2816.
59. Smith, B.D. (2011) Imatinib for chronic myeloid leukemia: the impact of its effectiveness and long-term side effects. *J. Natl Cancer Inst.*, **103**, 527–529.
60. Prunotto, M., Bacchetta, M., Jayaraman, S., Galloni, M., Van Eys, G., Gabbiani, G. and Bochaton-Piallat, M.L. (2007) Cytostatic drugs differentially affect phenotypic features of porcine coronary artery smooth muscle cell populations. *FEBS Lett.*, **581**, 5847–5851.
61. Ghofrani, H.A., Seeger, W. and Grimminger, F. (2005) Imatinib for the treatment of pulmonary arterial hypertension. *N. Engl. J. Med.*, **353**, 1412–1413.
62. Ten, F.H., Dumitrescu, D., Berghausen, E., Vantler, M., Caglayan, E. and Rosenkranz, S. (2012) Imatinib mesylate for the treatment of pulmonary arterial hypertension. *Expert Opin. Investig. Drugs*., **21**, 119–134.
63. Trache, A. and Lim, S.M. (2009) Integrated microscopy for real-time imaging of mechanotransduction studies in live cells. *J. Biomed. Opt.*, **14**, 034024.
64. Lim, S.M., Kreipe, B.A., Trzeciakowski, J., Dangott, L. and Trache, A. (2010) Extracellular matrix effect on RhoA signaling modulation in vascular smooth muscle cells. *Exp. Cell Res.*, **316**, 2833–2848.
65. Trache, A. and Meininger, G.A. (2008) Atomic force microscopy (AFM). *Curr. Protoc. Microbiol.*, Chapter 2, Unit.
66. Cao, Y., Ma, D. and Raabe, D. (2009) The use of flat punch indentation to determine the viscoelastic properties in the time and frequency domains of a soft layer bonded to a rigid substrate. *Acta Biomater.*, **5**, 240–248.
67. Trache, A., Trzeciakowski, J.P., Gardiner, L., Sun, Z., Muthuchamy, M., Guo, M., Yuan, S.Y. and Meininger, G.A. (2005) Histamine effects on endothelial cell fibronectin interaction studied by atomic force microscopy. *Biophys. J.*, **89**, 2888–2898.